

Interaction Between a Vibration Exciter and the Structure Under Test

Paulo S. Varoto and Leopoldo P. R. de Oliveira, University of São Paulo, São Carlos, Brazil

In order to obtain good quality data in modal and vibration testing, the experimentalist should pay attention to interactions that occur between the structure under test (SUT) and the instrumentation used in the test. Measurement errors can arise from a number of possible causes, including transducer mass loading effects, transverse stinger stiffness and exciter-SUT interactions. This article aims to study one of these sources of error, namely, the interaction between the electrodynamic exciter and the SUT. The effects caused by the shaker armature mass on the dynamics of the SUT are assessed in different testing conditions by using theoretical models and experimental analyses that include the exciter dynamic characteristics. Results from these studies indicate that the shaker interacts significantly with the structure under test and, under some circumstances, exciter dynamic effects can be accounted for in the process of improving measured data.

The electrodynamic vibration exciter has been intensively used in modal and vibration testing as a means to drive the SUT (Structure Under Test). In experimental modal analysis, a common practice is to attach the exciter to the SUT through a flexible stinger and a force transducer.¹ The stinger is used to transmit excitation signals to the SUT in a single direction, reducing secondary forms of excitation (e.g., bending moments) due to possible misalignments. The force transducer is used along with the exciter to measure the input force applied to the SUT. In vibration testing, the SUT is attached to the exciter table through a test fixture.² In this case, the SUT is driven by base excitation signals that are transmitted to the SUT through the test fixture. In this type of test it is common practice to employ a closed loop test procedure where the exciter's table is controlled so that a signal having a prescribed frequency content is applied to the SUT. In both cases, it is well known that the exciter interacts with the SUT and that in some circumstances, distortions due to the armature's dynamics can significantly alter measured data.

Exciter dynamics and its interactions with the SUT have been approached by several authors. Tomlinson² studied the interaction between the exciter and the SUT, paying special attention to the force dropout that occurs when the structure is excited in the vicinity of a structural natural frequency. This work also emphasizes the nonlinearity characteristics that arise from the electromagnetic field that is generated during the exciter working cycle. Olsen⁴ studied the effects of the armature's mass and suspension stiffness on measured data and pointed out that the armature's mass effects on the measured Frequency Response Functions (FRF) can be minimized by selecting an appropriate exciter for a given test. Rao⁶ followed the basic development by Olsen, but the dropout of the excitation force was analyzed in more detail. According to his work the dropout phenomenon is due primarily to mechanical interaction between the armature's mass and the structure and electromagnetic characteristics of the exciter coil circuit.

Exciter dynamics as well as its interactions with the SUT have been approached in various text books on modal and vibration testing. Ewins¹ formulated a simple dynamic model that explains the basic mechanical interaction between an exciter's armature and the SUT. The author draws attention to

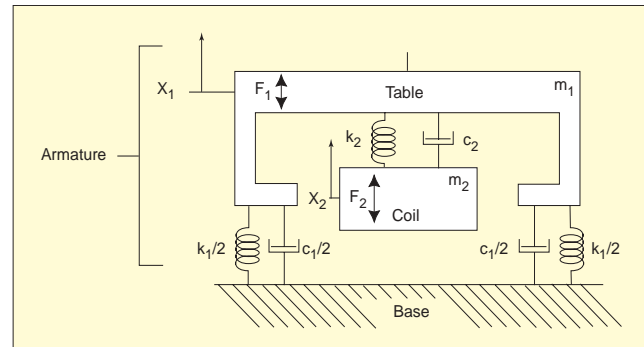


Figure 1. Armature 2 DOF dynamic model.

the fact that the excitation force must be directly measured during the test in order to obtain reliable FRF measurements. McConnell² developed an extensive study on exciter dynamics and its interaction with the SUT. In his work several analytical models were developed to explain mechanical interactions between the exciter and both free and grounded SUT. In addition, his work approached the electric characteristics of the exciter-power amplifier system during the test, showing the basic differences that occur when the power amplifier is used either in its voltage or current modes of operation. Maia⁹ also developed an interesting study on the subject by using simple dynamic models to model interactions between the exciter and grounded structures. An insightful paper was published by Lang⁵ where several simple tests are performed in order to evaluate exciter dynamics.

The objective of this work is to perform an experimental study on two different vibration exciters, attempting to evaluate some of their basic dynamic characteristics as well as their interaction with the test environment. The results obtained in this study and exhibited in this article constitute part of a project developed by one of the authors towards a degree in Mechanical Engineering.

Review of Theory

This section presents a review of important theoretical aspects that are concerned with the dynamics of a vibration exciter. The theoretical development that is described in this section is based on the work by McConnell² that presents a comprehensive analytical development of exciter dynamics. The theoretical development described here considers the exciter's armature dynamics as well as the electrodynamic relationships that are needed to explain an exciter's electric behavior and the two modes of operation of the power amplifier – the voltage and current modes.

Armature Dynamics. Figure 1 shows the armature dynamic model that consists of the table and the electromagnetic coil. In this case, the exciter base is considered to be rigidly attached to the floor. Hence, we have the 2 DOF (Degree of Freedom) mechanical system shown in Figure 1, where m_1 , k_1 and c_1 represent the table mass, stiffness and viscous damping and m_2 , k_2 and c_2 the spider mass, stiffness and viscous damping, respectively.

As described in McConnell,² the frequency domain accelerations $A_1(\omega)$ and $A_2(\omega)$ exhibited by the table and the coil, respectively, can be written in terms of the driving point and transfer acceleration FRFs, A_{11} , A_{12} and A_{22} , according to

Based on a paper presented at the 19th International Modal Analysis Conference, Kissimmee, FL, February 2001.

$$A_1 = \frac{A_{11}(\omega)}{m_a} F_1 + \frac{A_{12}(\omega)}{m_a} F_2 \quad (1)$$

$$A_2 = \frac{A_{21}(\omega)}{m_a} F_1 + \frac{A_{22}(\omega)}{m_a} F_2$$

where $A_{11}(\omega)$ is the table driving point FRF and $A_{12}(\omega) = A_{21}(\omega)$ is the transfer acceleration FRF. The armature's FRFs present in Eq. (1) represent important quantities since they give some useful information about armature behavior.

The driving point and transfer accelerances $A_{11}(\omega)$ and $A_{22}(\omega)$ are expressed as²

$$A_{11}(\omega) = \frac{m_a A_1}{F_1} = \frac{-r^2(1+M)(\beta^2 - r^2 + i\beta\eta_2)}{\Delta(r)} \quad (2)$$

$$A_{22}(\omega) = \frac{m_a A_2}{F_2} = \frac{-r^2(1+M)[(1+M\beta^2) - r^2 + i(\eta_1 + \beta M\eta_2)]}{\Delta(r)} \quad (3)$$

$$A_{12}(\omega) = \frac{m_a A_2}{F_2} = \frac{-r^2(1+M)(\beta^2 + i\beta\eta_2)}{\Delta(r)} \quad (4)$$

where the auxiliary variables appearing on Eqs. 2, 3 and 4 are defined as

$$\beta = \frac{\omega_{22}}{\omega_{11}} \quad M = \frac{m_{22}}{m_{11}} \quad (5)$$

$$\Delta(r) = \left[(1 + \beta^2 M) - r^2 + j2r(\zeta_1 + \zeta_2 \beta M) \right]^* \left[\beta^2 - r^2 + j2r\zeta_2 \beta \right] - \left[\beta^2 M \right] \left[\beta + j2r\zeta_2 \right]^2 \quad (6)$$

These three dimensionless acceleration FRFs are shown in Figure 2. They are identical as the dimensionless frequency ratio r ranges from 0.1 to 10. In this frequency range it is observed the existence of a natural frequency that is common to all FRFs and that it is the first resonance of the two DOF system. Above $r = 10$, the FRFs diverge and each one exhibits its own characteristics.

The coil's acceleration $A_{22}(\omega)$ decreases after $r = 10$ up to $r \approx 31.6$, where the table presents a dynamic absorber behavior for the coil. This acceleration then increases up to $r \approx 105$ (coil's resonance) and becomes constant. The table driving point acceleration $A_{11}(\omega)$ exhibits an antiresonance at $r = \beta = 100$ followed by its resonance at $r \approx 105$ and reaches a plateau of 1.1 (i.e., $1+M$) for higher frequencies ($r \gg 100$).

Finally, considering the table transfer acceleration $A_{12}(\omega)$, we have a resonance at $r \approx 105$ that decreases at a ratio of 40 dB/decade. This behavior shown by $A_{12}(\omega)$ clearly indicates that it is quite impossible to control the table after $r = 300$, since its dynamic response is more affected by external forces than by the coil's input. Therefore, the armature-coil system has an upper frequency limit for effective use of the exciter. In this case this frequency limit is given by²:

$$r_2 = \beta\sqrt{1+M} = \frac{\omega_{22}}{\omega_{11}} \sqrt{1+M} = \sqrt{\frac{k_2(m_1 + m_2)}{k_1 m_2}} \quad (7)$$

Electromechanical Model. Figure 3 shows the electromechanical model used by Olsem⁴ and McConnell² to describe the electromagnetic coupling on the armature-coil system. This electromechanical coupling is governed by several parameters: the coil resistance R , inductance L , input voltage signal $E(t)$ and the back electromagnetic voltage E_{bemf} . The equations that govern the mechanical and electrical systems shown in Figure 3 are, respectively, given as:

$$m_a \ddot{x} + c_a \dot{x} + k_a x = F_c(t) \quad (8)$$

$$RI + L\dot{I} + E_{bemf} = E(t) \quad (9)$$

where Eq. 9 was obtained using standard electric circuit relationships. However, the electromagnetic force $F_c(t)$, as well as the E_{bemf} voltage are hardly dependent on the exciter's mode of operation.² The subsequent sections show the basic equa-

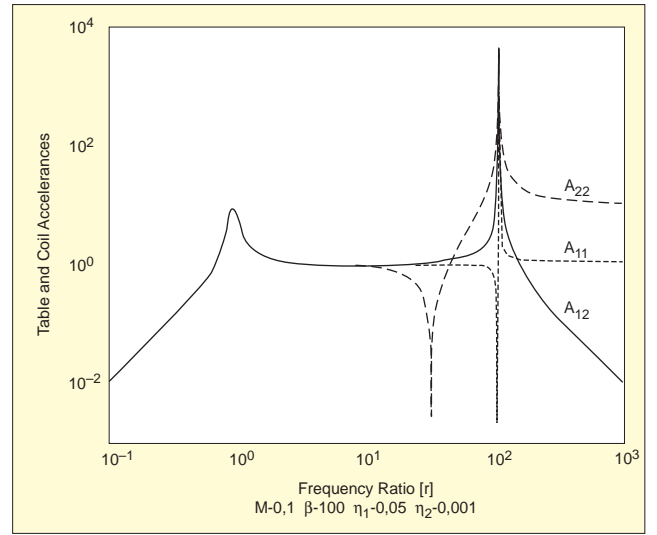


Figure 2. Dimensionless acceleration plot for an exciter armature.

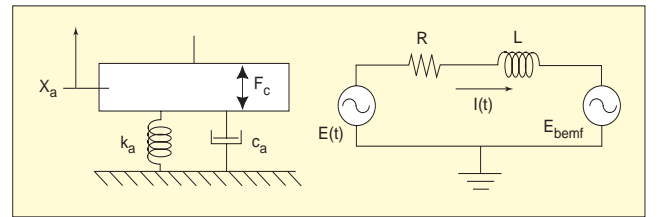


Figure 3. Exciter electromechanical model.

tions for both cases – voltage and current mode. The electrodynamic phenomenon that occurs on the exciter's circuits is mainly due to the interaction between the current and the armature motion in the exciter's electromagnetic field.

The Ampere law relates the electromagnetic force $F_c(t)$ and the current $I(t)$ through the coil, according to

$$F_c = (nBI)I = K_f I \quad (10)$$

where B is the magnetic field intensity generated by the current $I(t)$ through n coils, each one having length equal to l . The constant K_f is the "force-current constant" and is equal to (nBl) .

Tomlinson³ developed a theoretical model establishing a relationship between the magnetic field B and the coil position x given as:

$$B = \frac{dy}{dx} = B_0 \left[1 - \left(\frac{x + x_0}{x_{max}} \right)^2 \right] \quad (11)$$

where B_0 is the highest intensity that the field B reaches, x_0 is the armature initial position, x is its oscillation amplitude and x_{max} is the maximum amplitude. It can be verified yet by Equations 10 and 11 that the relationship between the force and the current is nonlinear:

$$F_c = nIB_0 \left[1 - \left(\frac{x + x_0}{x_{max}} \right)^2 \right] I \quad (12)$$

In addition, Lenz's law gives the relationship between the E_{bemf} and the armature's velocity as:

$$E_{bemf} = nBl\dot{x} = K_v \dot{x} = K_v \left[1 - \left(\frac{x + x_0}{x_{max}} \right)^2 \right] \dot{x} \quad (13)$$

It could be noticed from Eq. 13 that the E_{bemf} also presents a nonlinear factor proportional to the relationship between excitation amplitude and armature maximum amplitude and its velocity, i.e., the excitation frequency.³

Figure 4 shows the E_{bemf} behavior in terms of excitation amplitude and frequency. When the frequency is half of the original excitation frequency, the E_{bemf} drops to a new value that is half of the original one. The effects of the amplitude of oscil-

lation are related to the nonlinear behavior. The smaller the amplitude, the more linear the E_{bemf} variation.²

Power Amplifier – Modes of Operation. As stated earlier, the power amplifier has two modes of operation, the current and voltage modes, respectively. These modes establish the voltage versus current relationships during exciter operation. The basics of each mode of operation will be described.

In the current mode of operation, the relationship between the input voltage to the amplifier and its output current is given by an equation of the type

$$I(\omega) = G_i(\omega)V(\omega) \quad (14)$$

The frequency domain versions of Equations 8 and 9 are given as

$$(k_a - m_a\omega^2 + jc_a\omega)X = K_f I_0 \quad (15)$$

$$(R + jL\omega)I_0 + jK_v\omega X = E_0 \quad (16)$$

where I_0 and E_0 are reference amplitudes for the current and voltage, respectively. Notice that the simpler relationship between the E_{bemf} and the table's velocity (Eq. 13) is used in Eq. 16.

The dimensionless armature acceleration in the current mode is given by:

$$A(\omega) = \frac{m_a(-\omega^2 X)}{K_f I_0} = \frac{-r^2}{1 - r^2 + j2\zeta_a r} \quad (17)$$

where r is the dimensionless frequency ratio, now based on the armature natural frequency, and ζ_a is the armature viscous damping ratio.

Thus, the voltage needed to maintain the current magnitude is given as

$$E(\omega) = \frac{E_0}{R I_0} = 1 + j \left[\beta_1 + \frac{2\zeta_e}{1 - r^2 + j2\zeta_a r} \right] \quad (18)$$

where $\beta_1 = \omega_a / \omega_e$ and ω_a is the armature's natural frequency and ω_e is the break frequency:

$$\omega_e = \frac{R}{L} \quad (19)$$

The electromagnetic damping ratio ζ_e is given by:

$$\zeta_e = \frac{C_m}{2\sqrt{k_a m_a}} = \frac{K_v K_f}{2R\sqrt{k_a m_a}} \quad (20)$$

which is the result of the back emf current being dissipated by the coil circuit. It is important to remember that these equations are valid for low table amplitudes, which make the nonlinear terms vanish, as described by Tomlinson.

Similar to the current mode, the voltage mode of power amplifier operation can be modeled as a gain, constant in frequency up to a given cutoff frequency,² according to the following equation

$$E(\omega) = G_v(\omega)V(\omega) \quad (21)$$

where $G_v(\omega)$ is the amplifier gain, $V(\omega)$ and $E(\omega)$ are the amplifier's input and output voltages, respectively.

Following a similar procedure, the dimensionless armature acceleration in the voltage mode of operation is give as:

$$A(\omega) = \frac{m_a(\omega^2 X)}{K_f \left(\frac{E_0}{R} \right)} = \frac{-r^2}{1 - (1 + M_L)r^2 + j \left[2(\zeta_a + \zeta_e) + \beta(1 - r^2) \right] r} \quad (22)$$

where the dimensionless mass ratio $M_L = m_e / m_a$ and the inductive mass m_e is given by:

$$m_e = \frac{Lc_a}{R} \quad (23)$$

where it can be noticed from this last equation that the inductive mass is dependent on armature damping.

In order to gain additional insight to an exciter's dynamic behavior when operated in either the current or voltage modes, a simple simulation was performed with the physical parameters of an available vibration exciter. The exciter parameters

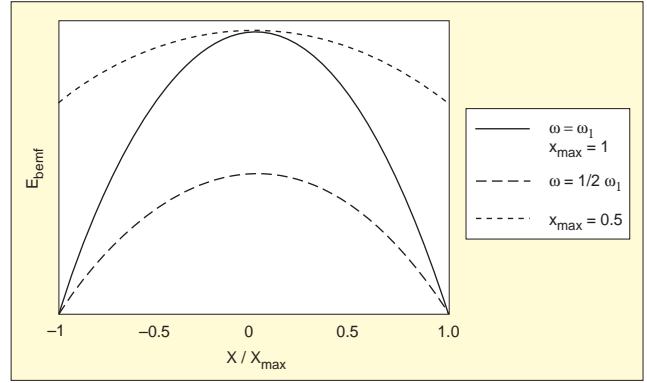


Figure 4. E_{bemf} behavior due to frequency and amplitude variation.

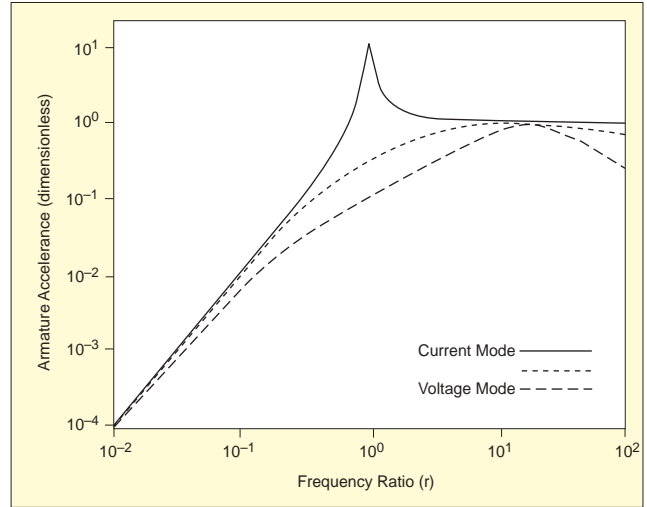


Figure 5. Dimensionless bare table acceleration.

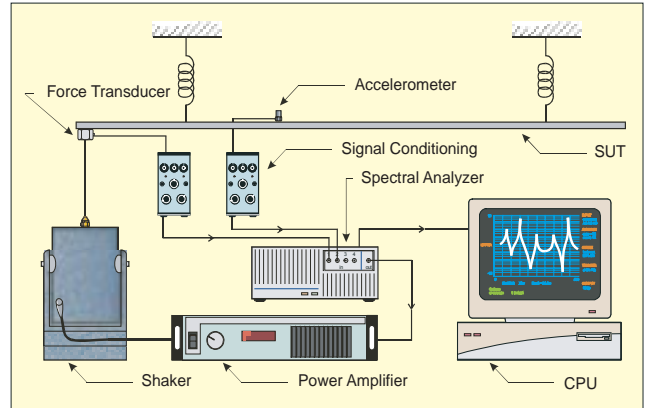


Figure 6. Test on free-free steel beam.

are shown below and correspond to a MB Dynamics Modal 50 vibration exciter. These parameters were obtained from the exciter's operating manual.

Force	111 N
Useful Displacement	25.4 mm
Maximum Displacement	27.9 mm
Shaker Mass	24.9 kg
Armature Mass	0.227 kg
Armature Axial Stiffness	2312 N/m
Coil Current (Max)	8.5 A (Low Impedance)
	4.2 A (High Impedance)
Coil Resistance	1.3 Ω (Low Impedance)
	5.2 Ω (High Impedance)

Figure 5 shows the bare armature acceleration FRF behavior for the current and voltage modes, according to Eqs. 17 and 22, where it shows the differences between the two modes of operation. In the current mode FRF (solid line), once the table

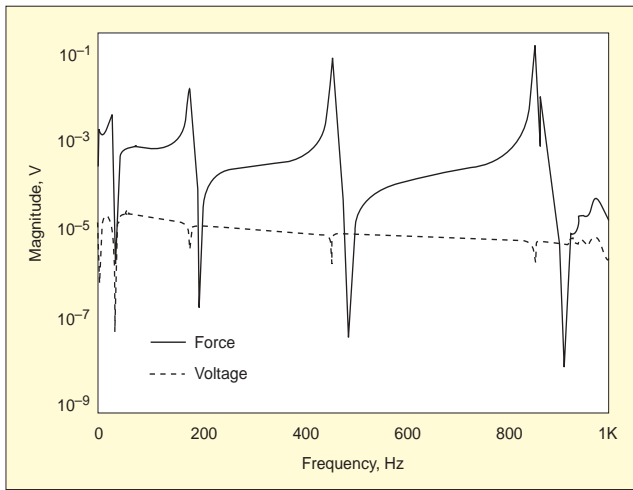


Figure 7. Force and current measurements for beam test.

passes through its mechanical resonance, the FRF amplitude becomes constant. In principle, this implies a reliable condition for exciter operation as stated by McConnell.² The other two FRFs depicted on Figure 5 correspond to the bare table FRF in the voltage mode of operation. There is a clear distinction between these FRFs when compared to the current mode FRF. The bare table resonance is severely damped in the voltage mode FRF, mostly due to high electrodynamic damping. Also, the two voltage mode FRFs shown in Figure 5 are different in the sense that they use different values for the coil resistance. It is seen that the smaller resistance yielded magnitudes closer to the current FRF for higher frequencies.

Experimental Results

This section presents some experimental results obtained from tests performed using two different exciters, a B&K 4812 with Power Amplifier B&K 2707 and a MB Dynamics Modal 50 with Power Amplifier SL500VCF. These tests were performed in order to get some practical understanding of the exciter's dynamic behavior as well as the interaction between the exciter and the SUT.

Results for Exciter-SUT Interaction. This section shows a sample among many results obtained in the developed project. The results shown here contain important features concerned with the exciter-SUT interaction.

Figure 6 shows the experimental setup used in one of the tests. This test used a cold-rolled steel beam (1000×25.4×6.25 mm) mounted directly on the MB Dynamics exciter table. A Kistler 912 force transducer was used to measure the input force to the beam and a B&K 4371 accelerometer was used to measure the beam's output acceleration. Hanning windows were used in both the input and output signals. The beam was excited with a random signal in the 0-1000 Hz frequency range. The SL500VCF power amplifier was adjusted to operate in the voltage mode. Figure 7 shows the results obtained for the input force to the beam and the voltage for the voltage mode of the power amplifier. Note that a dropout on the voltage values occurs at frequencies in the vicinity of the beam's ungrounded natural frequencies. These voltage dropouts coincide with the force dropout for the lower natural frequency, but deviate as frequency increases. Similar behavior was observed by McConnell² in numerically simulated results.

Figure 8a simultaneously shows a plot of a FRF of an aircraft wing structure and plots of the output acceleration and input force. These quantities were normalized so that they could be plotted on the same graph. These experimental results were obtained using the B&K exciter and power amplifier. This figure clearly shows that a given structural natural frequency (notice the dashed lines on Figure 8a) does not necessarily occur where the structure presents maximum values for the output ac-

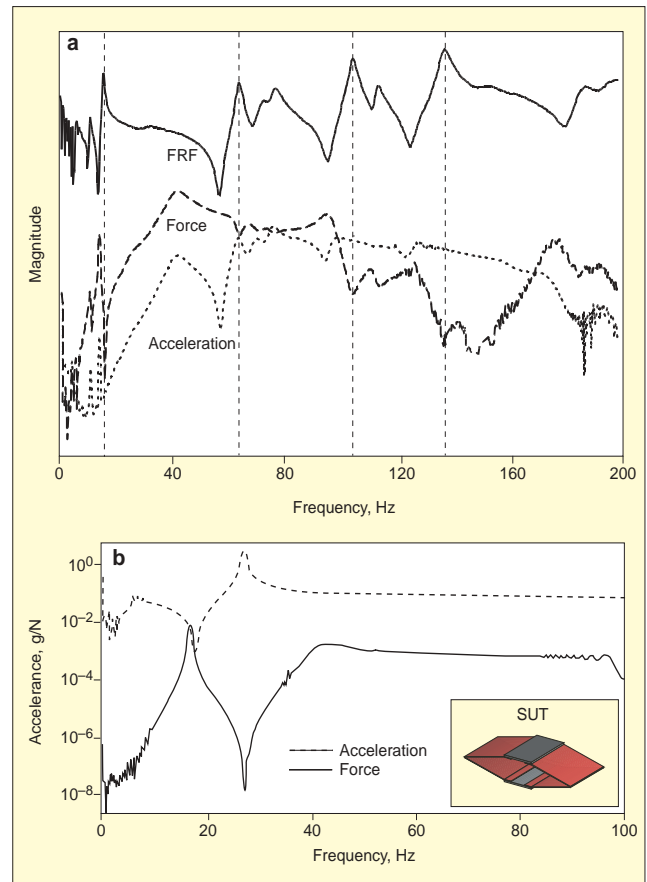


Figure 8. (a) FRF, acceleration and force measurements of an aircraft wing structure. (b) Force dropout in shaker testing.

celeration. Rather, they occur where the input force drops out to a minimum value. Again, the same observations were made by other authors.^{1,2,6} Figure 8b shows essentially the same behavior observed in Figure 8a. In this case, a simpler structure was used that contains a single natural frequency in the 0-100 Hz frequency range. Once again, the value of the structure's natural frequency and the frequency where the force dropouts occur are very close.

Figure 9 shows an acceleration FRF that was obtained using the B&K 4812 exciter with random excitation and the PCB impact hammer. The experimental results are compared with results obtained from an analytical model of the SUT. The main feature of this test is that even though two different excitation mechanisms were employed to drive the test structure, the same value is obtained for the natural frequency (about 27.3 Hz), as shown in Figure 9. While not shown here, recall that in impact testing the input force auto spectral density is constant (or almost constant) in the tested frequency range. Figure 9 still shows a rigid body natural frequency (about 5 Hz) due to the SUT suspension system that is not present in the ideal simulated FRF. Although the natural frequencies are essentially the same for both testing conditions, there is a mismatch in the anti-resonance that occurs at a frequency close to 20 Hz. An interesting fact can be observed in the anti-resonance obtained in the exciter test. The anti-resonance (dotted line) occurs at approximately 18 Hz, a value that is slightly lower than the anti-resonance value for the hammer test. The armature's suspension stiffness and mass values for the B&K exciter are about $K_a = 21$ kN/m and $m_a = 0.454$ kg, as stated in the operating manual. On the other hand, the SUT has a mass of $m = 1.046$ kg. These values allow us to get the frequency $\omega = [k_a/(m+m_a)]^{1/2} = 118.3$ rad/s = 18.83 Hz!

Hence, the anti-resonance observed in Figure 9 is essentially the natural frequency of the armature-SUT system, but in

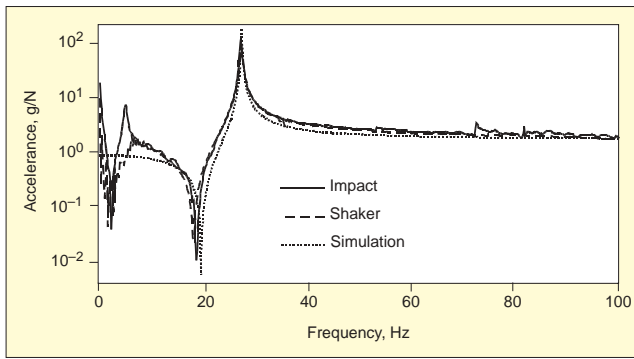


Figure 9. Analytical and experimental FRFs.

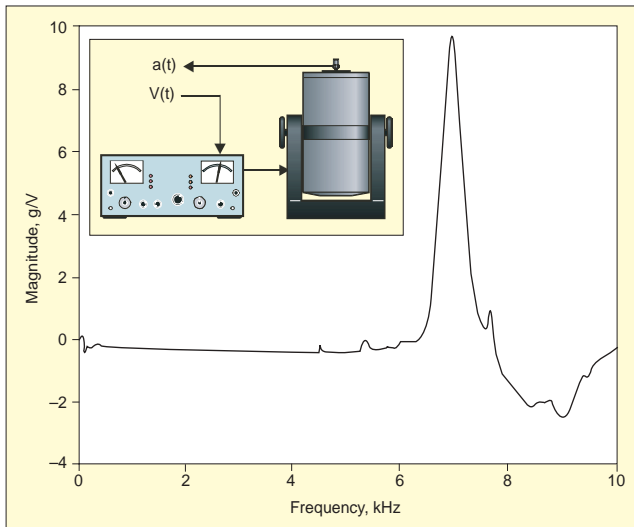


Figure 10. B&K 4812 bare table FRF.

the SUT response it appears as a dynamic absorber action. Finally, the anti-resonance amplitude obtained with the exciter testing is higher than that obtained with impact testing. This result, along with the frequency mismatch already discussed, indicates a clear exciter-SUT interaction.

Results for Armature's Dynamics. This section shows a sample of experimental results that were obtained in tests that aimed to determine an exciter's basic dynamic behavior.

Figure 10 depicts the B&K 4812 exciter's bare table acceleration FRF. This result was obtained by measuring the exciter's table acceleration using the B&K 4371 accelerometer while the excitation frequency was varied in the 0-10,000 Hz frequency range. The acceleration values were normalized by the input voltage from the signal generator. The result shown in Figure 10 exhibits a peak frequency at 6885 Hz, while the exciter operating manual gives 7200 Hz as the bare table natural frequency. Hence, although there is a difference of about 4%, this test was considered effective in obtaining the bare table natural frequency.

Figure 11 shows results obtained when the shaker table is impacted by an instrumented hammer and the table acceleration is measured in two different conditions. The solid line shows the FRF that was obtained when the power amplifier is turned off and the dashed line shows the same FRF with the power amplifier turned on. In this condition no excitation signals were sent to the shaker. The only difference between these test conditions is that in the first case the exciter's internal circuits are not electrically energized while in the second the power amplifier is turned on and thus electrical energy is flowing through the coil circuit. The results shown in Figure 11 are suitable for observing the effects of the additional damping and possibly stiffness induced by the coil electromagnetic field that is established during exciter operation.

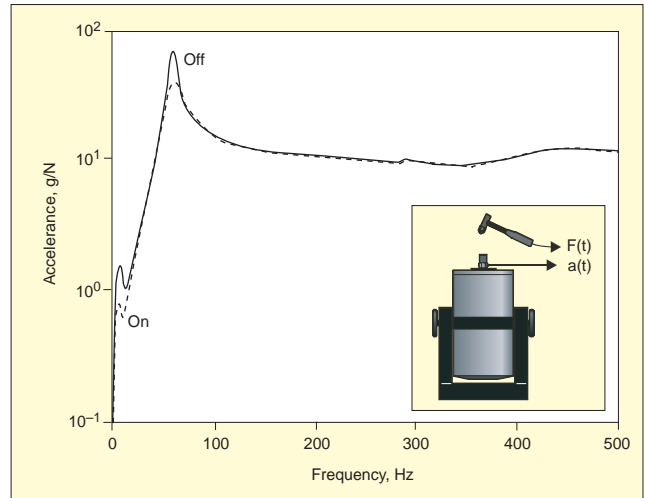


Figure 11. Electromagnetic damping.

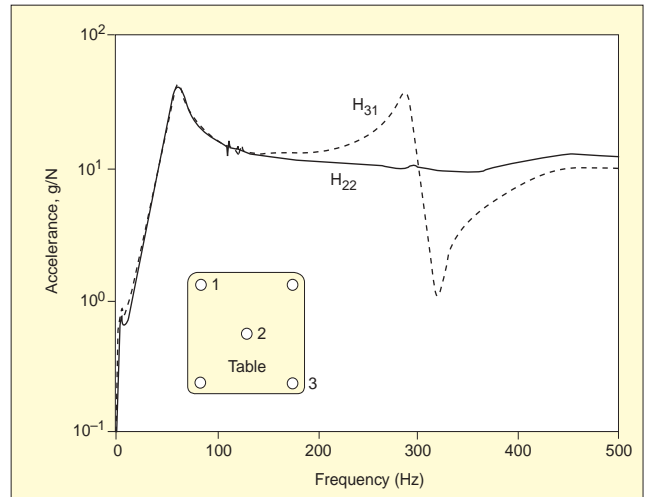


Figure 12. Effects of rocking motion on table.

Figure 12 shows results that were obtained by impacting the B&K 4812 bare table. The aim of this test was to investigate eventual rocking motions presented by the exciter's table. For this purpose, two acceleration FRFs were gathered, as shown in Figure 12. Accelerance $H_{22}(\omega)$ is nearly a driving point FRF, where the exciter's table was impacted at location 2 (Figure 12) and the response was measured close to the table center. The plot of $H_{22}(\omega)$ shows a single natural frequency that corresponds to the armature's suspension natural frequency. The plot for acceleration $H_{31}(\omega)$ was obtained by impacting the table at location 1 and measuring the acceleration at location 3. Both acceleration FRFs show essentially the same behavior from 0-120 Hz, after which they differ significantly. While $H_{22}(\omega)$ is nearly constant up to the end of the frequency bandwidth, $H_{31}(\omega)$ exhibits a second resonant peak at approximately 280 Hz followed by a valley at 330 Hz. This second natural frequency indicates that a strong rocking motion is taking place on the shaker's table when the impact is applied at a point that does not coincide with the armature's vertical axis. Some other interesting results not reported here on damping differences were also observed. This test tells us something about running base excitation tests in the SUT that are not symmetrical with respect to the armature's vertical axis!

A simple but interesting test was performed with the MB Dynamics Modal 50 exciter in order to get an estimate of the armature's suspension damping ratio. A small mass with a miniature accelerometer was mounted on the top of the exciter table. With the power amplifier off, the armature was plucked and the free decay acceleration was mea-

sured. These data were used to estimate the damping factor through logarithmic decrement, resulting in a value of 2.6% for the armature's damping ratio.

Summary and Conclusions

This article presents an experimental study on exciter dynamic behavior as well as on its interaction with the structure under test. Several tests were performed and interesting characteristics were observed. The major conclusion from this work is that the exciter represents an effective excitation mechanism. However, it should be used with care, since it interacts with the test environment. Also, the two power amplifier modes can distort test results.

Acknowledgements

The authors kindly acknowledge the financial support provided by FAPESP (grant # 99/0229-6) to Mr. Leopoldo P. R. de Oliveira during the development of the project and to EESC-USP for providing the necessary laboratory facilities.

References

1. Ewins, D. J., *Modal Testing: Theory and Practice*, RPS, London, 1984.
2. McConnell, K. G., *Vibration Testing: Theory and Practice*, John Wiley & Sons, NY, 1995.
3. Tomlinson, G. R., "Force Distortion in Resonance Testing of Structures with Electrodynamic Vibration Exciters," *Journal of Sound and Vibration*, Vol. 63, No. 3, 1979, pp. 337-350.
4. Olsem, N. L., "Using and Understanding Electrodynamic Shakers in Modal Applications," Proceedings of the 4th International Modal Analysis Conference, IMAC 1986, Vol. 2, pp. 1160-1167.
5. Lang, G. F., "ElectroDynamic Shaker Fundamentals," *Sound and Vibration*, April, 1997. pp. 14-25.
6. Rao, D. K., "Electrodynamic Interaction Between a Resonating Structure and an Exciter," Proceedings of the 5th International Modal Analysis Conference, IMAC 1987, Vol. 2, pp. 1142-1150.
7. Instruction Manual, B&K Vibration Exciter System V, 1974.
8. Instruction Manual, MB Dynamics Modal 50A Vibration Exciter, 2000.
9. Maia, N. M. M., Silva, J., *Theoretical and Experimental Modal Analysis*, RSP, 1997. 

The authors may be contacted at: varoto@sc.usp.br and leopro@sc.usp.br.